J Appl Electrochem (2012) 42:333–339
DOI 10.1007/s10800-012-0401-9

ORIGINAL PAPER

Electrochemical deposition of Co–Sb thin films on nanostructured gold

Ruxandra Vidu · Simon Li · Dat V. Quach · Pieter Stroeve

Received: 14 October 2011 / Accepted: 15 March 2012 / Published online: 30 March 2012

Abstract The electrochemical behavior of the Co–Sb system on Au substrate during cyclic voltammetry and potentiostatic deposition was investigated. Electrochemical behavior of Co and Sb was studied and compared to the Co–Sb system. At a negative potential (−0.9 V vs. Ag/AgCl) the electrochemical behavior of this binary system was similar to that of individual Co and Sb combined. For more negative vertex potentials (e.g., −1.2 V vs. Ag/AgCl), results from cyclic voltammetry have shown the presence of a new compound different from Co and Sb which could only be detected at slow sweep rate. The deposition performed at constant potentials between −1.0 and −1.2 V have resulted in films that were made of $CoSb_3$ and Sb as indicated by XRD. Surface film studied by SEM and EDS has shown morphological and compositional non-uniformities caused by hydrogen evolution.

Keywords Thermoelectric · Electrochemical deposition · Cyclic voltammetry · Thin film · Skutterudite · Cobalt triantimonide

1 Introduction

Thermoelectric materials directly convert heat to electricity based on the Seebeck effect and are commonly used in thermal management of computer chips or to generate electricity from waste heat. In addition, the Peltier effect can cause heat to flow from a cold side to a hot side when an electrical current is passed through the thermoelectric, thus allowing the material to be used in environmentally friendly refrigeration systems. The performance of a thermoelectric device is related to the dimensionless figure of merit (ZT) of the material:

$$ZT = \frac{S^2 \sigma T}{\kappa}$$

where S is the Seebeck coefficient, σ is electrical conductivity, κ is thermal conductivity and T is temperature. In principle, the figure of merit (and ultimately the efficiency of a thermoelectric device) can be improved by increasing Seebeck coefficient and electrical conductivity while keeping thermal conductivity low. These thermoelectric properties are, however, interrelated and hard to be independently controlled. Although the usual low efficiency of thermoelectric devices makes this type of materials less competitive in the current energy market [1], theoretical predictions and recent experimental results exploiting nanoscale effects in thin films, nanowires and superlattices give unprecedentedly high figure of merit and promise an improved efficiency for thermoelectric devices [2–5].

Cobalt triantimonide ($CoSb_3$) belongs to a group of materials called skutterudites indicated by MX_3 where M is a metal atom and X is a pnictide atom. These materials crystallize in a body-centered cubic structure whose unit cell consists of eight corner-shared MX_6 octahedra, which produce a large cage occupying the center position. Rattlers from large atoms such as La, Ce and other rare earths can be introduced to the open cage of skutterudites in order to further reduce the lattice thermal conductivity. Even though they tend to have good thermoelectric properties at intermediate temperatures (400–600 °C), the focus of most

R. Vidu (✉)
NanoRIS, Sacramento, CA, USA
e-mail: ruxandra@nanoris.net

S. Li · D. V. Quach · P. Stroeve
Department of Chemical Engineering & Materials Science, University of California, Davis, Davis, CA, USA

research on skutterudites has been on bulk materials [6–8]. The low-dimensional approach has not been fully explored for these types of compounds.

Thin films and nanowires of $CoSb_3$ have been prepared by several different techniques including pulsed laser deposition [9] and electrochemical deposition [10–12]. Electrochemistry is an inexpensive and versatile method to form nanostructured elements, composites, and thin films. Additionally, electrodeposition is performed at or near room temperature, which is considered low temperature deposition for compound semiconductors. Low temperature deposition is desirable for avoiding heat-induced interdiffusion of adjacent layers of a structure. Electrodeposition also promotes conformal growth on surfaces other than flat, and it is generally a low cost methodology. The most important reason for pursuing electrodeposition as a thin film formation methodology for compound semiconductors, is that some compounds and structures might be formed electrochemically which are not accessible by standard methods. Also doping is achievable in a one-step deposition process concomitantly with nanowire growth. These characteristics make the electrochemical deposition the method of choice for large scale production of many advanced nanostructured materials at low cost. Although the electrodeposition of cobalt on gold [13] and the electrodeposition of antimony on gold [14] have been subjects of many studies in the past, very few papers report on electrochemical deposition of $CoSb_3$.

Standard electrode potentials of antimony and cobalt are 0.212 and −0.277 V respectively, and the rather large potential difference (0.49 V) makes co-deposition of these metals from aqueous solutions of simple salts impractical. Fortunately, the introduction of metal complexes in the solution can bring the deposition potentials of these two metals closer. By adding citrate ions to the salt solution of Co^{2+} and Sb^{3+}, Sadana [15] was able to bring the potential difference down to 0.16 V. They managed to develop films of Co–Sb alloys with various compositions, although the formation of $CoSb_3$ compound was not mentioned in this study.

Behnke et al. [12] has further improved the above method by applying pulsed voltage during deposition. When the potential was below the antimony deposition potential but still above that of cobalt, a thin layer of antimony was deposited on the substrate. When the potential was further reduced below that of the cobalt deposition potential, both antimony and cobalt were deposited. By cycling between these two potential values and controlling the deposition time at each potential, Behnke et al. [12] were able to produce nanowires with Co:Sb $\approx$ 1:3. Due to the nature of the layer deposition, a post-deposition annealing was required so that Co and Sb on adjacent layers could react and form $CoSb_3$. After annealing in vacuum for 24 h at 400 °C, the samples contained polycrystalline $CoSb_3$ and probably an amorphous phase with some antimony deficiency.

Only recently, Chen et al. [10] reported a study on electrochemical synthesis of $CoSb_3$ nanowires in alumina template from a solution of SbO^+, Co^{2+}, and tartaric acid. It was found that the stoichiometry of the product was very sensitive to the pH value, and the 1:3 ratio of Co:Sb was obtained at a pH value of 2.5 by adding a small amount of HCl to the solution. During the co-deposition process, nucleation and growth of $CoSb_3$ occurred quickly to form nanowires that had a preferred (420) orientation.

In this proposed work, we will address the main challenge of the electrochemical deposition process which is the disparate reduction potential of Co(II) and Sb(III). Recently, we have reported on the growth of $CoSb_3$ nanowires by electrochemical deposition [16]. This article presents a detailed study on the electrochemistry of thin films of Co–Sb during the co-deposition of cobalt and antimony on nanostructured gold substrates. We use Au films on polycarbonate track-etched (PCTE) membranes in our research because the surface is nanostructured and has features that are similar to those used in template synthesis of nanowires.

2 Experimental methods

Solutions containing cobalt and antimony were prepared by dissolving 0.003 M Sb_2O_3 (99.99 %) and 0.172 M $CoSO_4{\cdot}7H_2O$ (>99 %) in aqueous solutions containing 0.125 M $C_6H_7KO_7$ (potassium citrate monobasic) (>99.0 %) and 0.196 M and $C_6H_8O_7$ (citric acid) (>99.5 %). All chemicals were purchased from Sigma-Aldrich. Deionized water (Milli Q 18-MΩ) was used for preparing solutions and for rinsing. The solution was purged with N_2 for at least 15 min before experimentation.

Gold sputtered PCTE membranes (GE Water & Process Technologies, PA, USA) were used as a substrate for deposition. The rough side of the PCTE membranes was first sputtered with Au using a SEM sputtering device for 4 min. A piece of double sided copper tape was then placed in contact with the Au-coated side of the membrane. Finally the two pieces were sandwiched between two single sided plastic tapes with a circular cut-out, exposing Au to the electrolyte. The circular cut-out had an approximate area of 0.3846 cm^2 with a pore size of 400 nm and pore density of 1×10^8 pores cm^{-2}. A diagram of the set-up is shown in Fig. 1.

A conventional three-electrode setup including a computer-controlled bi-potentiostat (Model AFCBP1, Pine Instrument Company) was used for both cyclic voltammetry (CV) and potentiostatic cathodic electrodeposition.

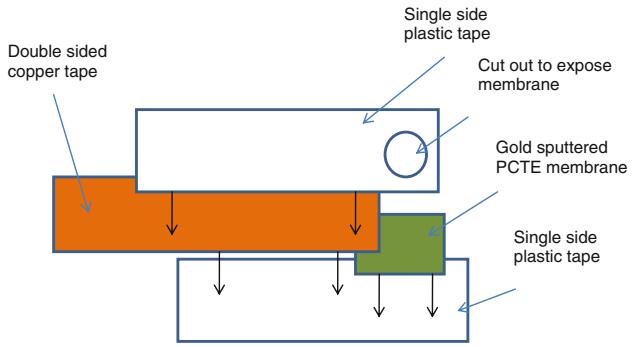

Fig. 1 Schematic of sample set-up for CV and electrochemical deposition experiments

The counter electrode was an Au wire and the reference electrode was Ag/AgCl electrode (3 M NaCl). The potentials presented here are relative to Ag/AgCl (0.194 V vs. standard hydrogen electrode). The Aftermath software (National Instruments, TX, USA) was used to control the computer.

CV experiments were performed from 0.5 to a vertex potential that varied from −0.9 to −1.2 V at different rates ranging from 5 to 100 mV s^{-1} for solutions containing antimony only, cobalt only and both cobalt and antimony ions. These provide useful information on the deposition of Co and Sb and their interaction. Another set of CV experiments similar to the aforementioned experiment, but with different hold time from 0 to 300 s at various potentials in the deposition range, were carried out in order to study the growth mechanism of thin films.

3 Results and discussion

3.1 Electrochemical treatment of Au surface

A series of CVs were performed in 50 mM H_2SO_4 in order to clean the Au surface and create the same surface condition before each experiment. The sulfuric acid solution was prepared from Sigma-Aldrich. For the cleaning purpose, the following CVs were performed: (1) the first CV was performed from 0 to 1.5 V at 50 mV s^{-1} for one cycle, (2) a second CV set was done from 0 to 0.9 V at 50 mV s^{-1} for 10 cycles, (3) an electrochemical treatment of the surface was done at 0.7 V for 15 min, and (4) a final CV from 0 to 1.5 V at 50 mV s^{-1} for one cycle was recorded afterwards.

During electrochemical treatment, Au surface atoms rearrange themselves by surface diffusion, and this process results in improved surface quality and reproducibility of experiments [17–23]. Cyclic voltammograms of Au in 50 mM H_2SO_4, before and after the electrochemical treatment were presented somewhere else [16]. Oxidation peaks shift and become sharper after electrochemical treatment. This shift in oxidation peaks is a signature of the surface rearrangement which can occur due to surface diffusion of Au atoms under applied potentials [20, 21, 24].

3.2 CV with varying sweep rate

3.2.1 Antimony deposition

Cyclic voltammograms of Au in a 0.003 M Sb_2O_3 + 0.125 M $C_6H_7KO_7$ + 0.196 M $C_6H_8O_7$ aqueous solution are shown in Fig. 2. The CV has a distinctive reduction peak around −0.1 V (D_1) that may be related to diffusion species or adsorbed species (i.e., underpotential (UPD) process). UPD occurs in those systems where the attraction between depositing atoms and the substrate is stronger than the attraction among the depositing atoms. That is why UPD takes place at potentials more positive than the Nernst potential. UPD was reported for Sb on Au single crystals [25]. In the Sb–Au system, the UPD process occurs after the irreversible reduction of the absorbed SbO^+. In

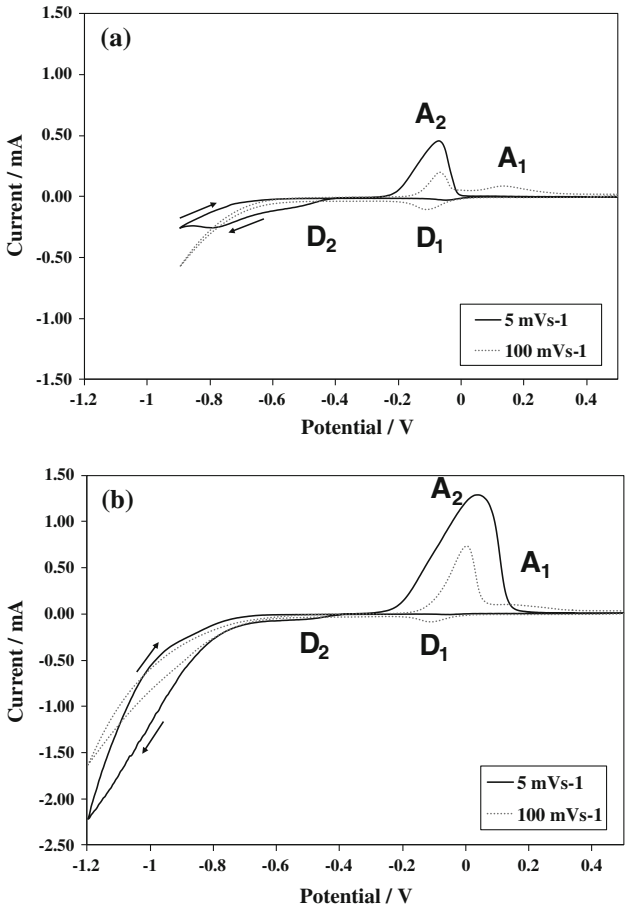

Fig. 2 CV on 400-nm Au in 0.003 M Sb_2O_3 + 0.125 M $C_6H_7KO_7$ + 0.196 M $C_6H_8O_7$ aqueous solution at 5 and 100 mV s^{-1} from (**a**) 0.5 to −0.9 V and (**b**) 0.5 to −1.2 V

addition, the absorption of SbO^+ is so strong that the Au surface is covered with a partially filled monolayer of SbO^+ as soon as the electrode is immersed in electrolyte [14, 25]. Scanning electron microscopy (SEM) has also identified the formation of a compound at the Au–Sb interface involving at least two top layers of the Au surface [8], which proves furthermore the existence of strong interactions in the Au–Sb system.

Therefore, the interpretation of the CV is complicated by other processes that precede or occur simultaneously with Sb thin film [8, 14, 25]. Although peak D_1 can be seen at all sweep rates, it is more easily detected at higher sweep rates. To make sure that the oxidation peak A_1 in a reverse scan corresponds to the deposition peak D_1, we have run a CV from 0.5 to −0.3 V and back to 0.5 V (not shown). In this case, only the A_1 and D_1 peaks were shown in the CV. Deposition of Sb takes place at more negative potentials, starting around −0.4 V (D_2), where hydrogen evolution is also observed. The deposition of Sb and hydrogen evolution become more significant at potentials below ∼−0.5 V.

3.2.2 Cobalt deposition

Figure 3 shows the CV results of Au in a 0.172 M $CoSO_4$ + 0.125 M $C_6H_7KO_7$ + 0.196 M $C_6H_8O_7$ aqueous solution. The sharp peak D at the end of CV indicates that Co deposition facilitates more hydrogen evolution than Sb deposition. This is consistent with literature data where hydrogen evolution is more favored on a Co surface compared to a Sb surface [26]. Also, the oxidation peak A depends on the position of the negative vertex potential. At low vertex potential (i.e., −0.9 V), the oxidation peak A is strongly shifted to positive potentials as the sweep rate decreases. At more negative vertex potential (i.e., −1.2 V), the oxidation peak A is slightly shifted to negative potentials as the sweep rate decreases. The intricate shift in peak potential with the sweep rate indicates a more complex interface process compared with a simple deposition process and may be due to the various phases of Co that may be formed on the surface: hcp or fcc. Bubendorf et al. [27] determined that the structure of electrodeposited Co thin films is dependent on pH and overpotential. At a pH of 4 and a high overpotential, an island growth of crystallized hcp Co was observed, whereas other conditions lead to continuous films containing larger fractions of fcc. The existence of various Co phases on the surface formed at a given overpotential, may explain the shift in stripping potential *A* observed in our particular system.

Cyclic voltammograms for this system exhibit a crossover between the cathodic and anodic branches, which is characteristic to the formation of nuclei on the substrate [28–30]. To help understand the CV scan, forward and reverse scan arrows are shown in the cyclic voltammograms

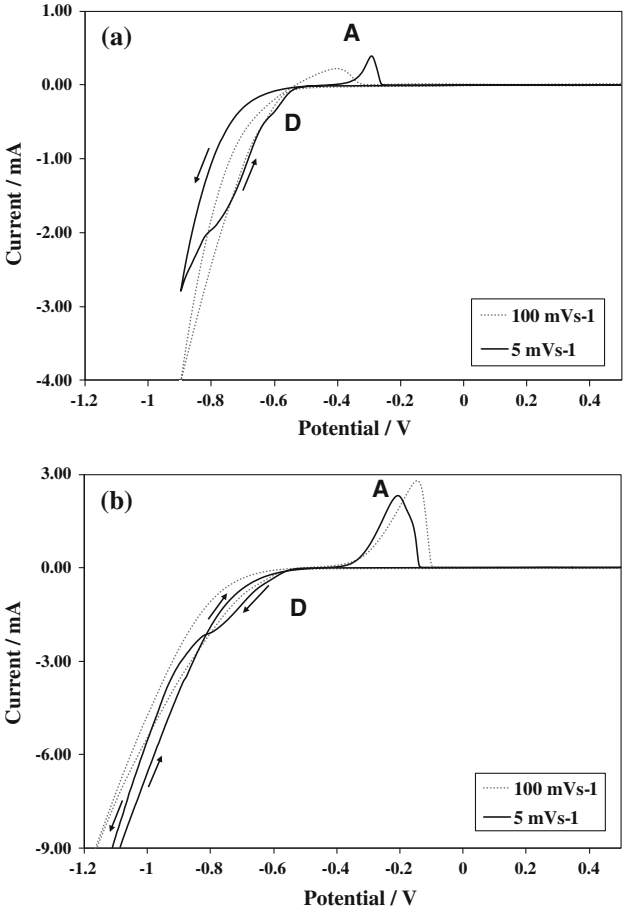

Fig. 3 CV on 400-nm Au in 0.172 M $CoSO_4$ + 0.125 M $C_6H_7KO_7$ + 0.196 M $C_6H_8O_7$ aqueous solution at 5 and 100 mV s^{-1} from (**a**) 0.5 to −0.9 V and (**b**) 0.5 to −1.2 V

with crossovers, i.e., Figs. 3 and 4. Typically, deposition of metal ions on a foreign substrate (e.g., Co^{2+}/Au) in a forward CV scan takes place at a potential more negative than the potential corresponding to the deposition on a same substrate (e.g., Co^{2+}/Co), because an overpotential is required by nucleation. In the reverse CV scan, the oxidation of the deposit takes place at a potential that is close to the metal/metal ion equilibrium potential (e.g., Co/Co^{+2}), causing the crossover in the CV. The noticeable crossover observed at −0.8 V in Fig. 3b demonstrates that cobalt deposition proceeds via nucleation and growth.

3.2.3 Co-deposition of cobalt and antimony

CV scans recorded for Au in a solution containing both cobalt and antimony ions are shown in Fig. 4. The shift and increase in magnitude of the peaks are observed with decreasing sweep rate, which is an indication of compound formation or surface alloying with Au atoms [18, 22]. For all sweep rates and vertex potentials, the first layer deposited on Au is Sb, seen as peak D_1, which is followed

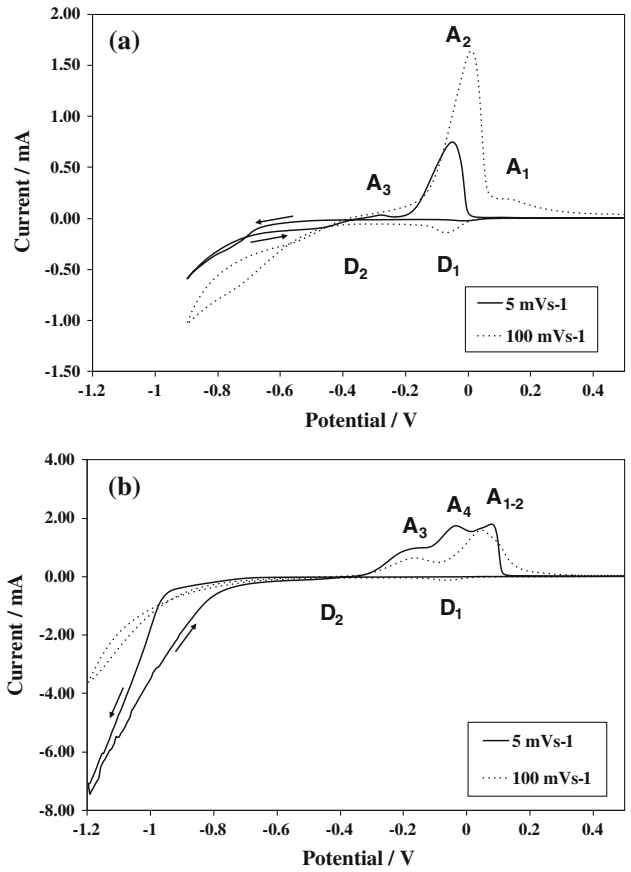

Fig. 4 CV of Au surface in 0.003 M Sb_2O_3 + 0.172 M $CoSO_4$ + 0.125 M $C_6H_7KO_7$ + 0.196 M $C_6H_8O_7$ aqueous solution (**a**) from 0.5 to −0.9 V and (**b**) from 0.5 to −1.2 V. For explanation of the peaks see text

by Co and Sb co-deposition. Hydrogen evolution was observed to interfere with Co–Sb film deposition at more negative potentials.

For less negative vertex potential (−0.9 V) the reverse scan showed quite distinctive peaks from Co (A_3), Sb (A_2 and A_1). This is similar to a CV obtained by superimposing Fig. 2a on Fig. 3a, where no clear interaction between Co and Sb was noticed. However, the situation changes as the vertex potential is set to more negative potential.

At a vertex potential of −1.2 V, besides the peaks for Co (A_3) and Sb ($A_{1\text{-}2}$) stripping, a new oxidation peak (peak A_4) was observed, especially at slower sweep rate (e.g., 5 mV s^{-1}). We believe that this peak is different from peak A_2 in Fig. 4a because it has a different shape and it precedes the Sb striping (peak $A_{1–2}$). This peak was attributed to the interaction between Co and Sb but was not observed at a sweep rate of 100 mV s^{-1}, suggesting that the formation of a Co–Sb phase was a slow process that occurred at high overpotential.

The shift in stripping peak potential A_2 associated with Sb stripping in Fig. 2, peak A associated with Co stripping in Fig. 3, and peak A_3 in Fig. 4 is shown in Fig. 5. The stripping of Co–Sb phase shows a peak that shifts with the sweep rate in a similar way as the single-element phase. For vertex negative potential of −0.9 V, the stripping of the Sb-rich Co–Sb phase behaves similar to the Sb-only system, while the stripping of the Co-rich Co–Sb phase (vertex potential of −1.2 V) behaves similar to the Co-only system. Also, the proximity of the peak shift of Co–Sb phase to the peak shift for Co (Fig. 5a) and Sb (Fig. 5b) is worth mentioning, which suggests that peak A_4 in Fig. 4b is different from peak A_2 in Fig. 4a. The appearance of the new oxidation peak A_4 indicates that the Co–Sb compound is stripped as a phase instead of individual elements. The XRD of the deposit obtained at −1.2 V for 2 h confirms the presence of a new phase ($CoSb_3$), whereas the film obtained at −1.0 V for 2 h shows mainly crystalline Sb (Fig. 6). Cobalt probably exists in amorphous phase and cannot be detected by XRD, not even at −1.2 V.

3.3 Potentiostatic deposition

Potentiostatic experiments have been performed to understand the growth of thin films. Figure 7 shows CVs recorded by sweeping the potential from 0.5 V to various

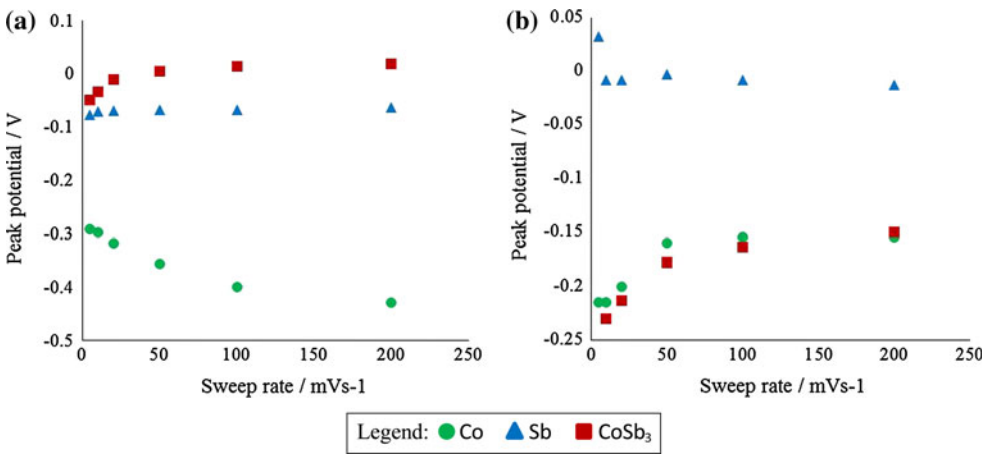

Fig. 5 Variation of desorption peaks with the sweep rate, when the negative vertex potential was set at −0.9 V (**a**) and −1.2 V (**b**)

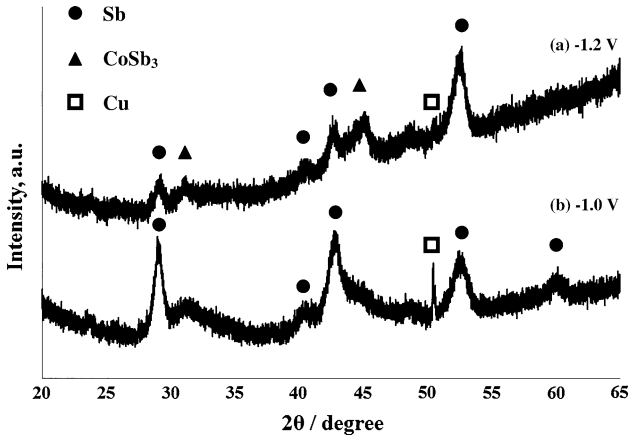

Fig. 6 X-ray diffraction patterns of Co–Sb films deposited for 2 h at (*a*) −1.2 V and (*b*) −1.0 V

deposition potentials (i.e., −0.9, −1.0, −1.1, and −1.2 V), holding the potential for various deposition times (from 0 s to 300 s) and then recording again the CV during the stripping of the deposit. Note that Fig. 8 only shows two times: 5 and 300 s, which represent the gradual transition from 5 to 300 s. At a deposition time of 5 s, the cobalt oxidation peak A (around −0.25 V) at less negative deposition potentials is small compared to the antimony oxidation peak B (from 0 to 0.3 V). As more negative potentials are applied however, the contents of both cobalt and antimony (peaks A and B) increase, with cobalt increasing at a faster rate than antimony. This observation is consistent with an EDS analysis that we have previously reported for Co–Sb co-deposition [16]. Consequently, deposition at a more negative potential increases the rate of cobalt deposition much faster than for Sb deposition. When the deposition is performed at more negative potentials, peak B associated with Sb stripping becomes asymmetrically wider and shifts to the right. At −1.2 V deposition for 5 s, another peak becomes apparent under peak B (Fig. 7d), which is associated with the formation of the $CoSb_3$ compound. At longer deposition times, peaks A and B tend to merge into one broad peak, making it practically impossible to differentiate among surface phases.

The SEM images of the Co–Sb film surface obtained at −1.1 V for 20 min are shown in Fig. 8. Similar morphologies were obtained for all films deposited between −1.0 and −1.2 V. The Co–Sb film covers the entire nanostructured Au template surface but the morphology and the composition of the film are not uniform. There are large Co-rich areas having a smooth surface along with large Sb-rich areas having a rough, cauliflower-type morphology. This particular surface feature with local variation in

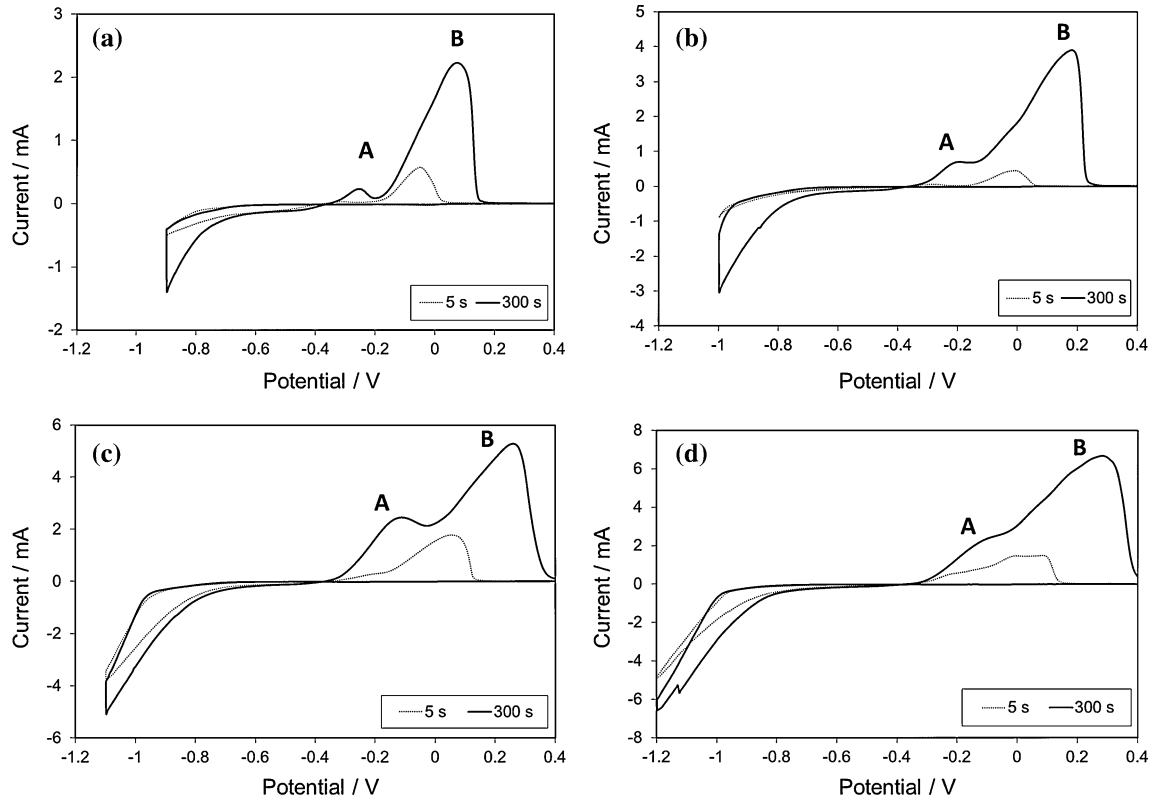

Fig. 7 CV on 400-nm Au template in 0.003 M Sb_2O_3 + 0.172 M $CoSO_4{\cdot}7H_2O$ + 0.125 M $C_6H_7KO_7$ + 0.196 M $C_6H_8O_7$ aqueous solution at 5 mV s^{-1} with various hold times at −0.9 V (**a**), −1.0 V (**b**), −1.1 V (**c**), and −1.2 V (**d**)

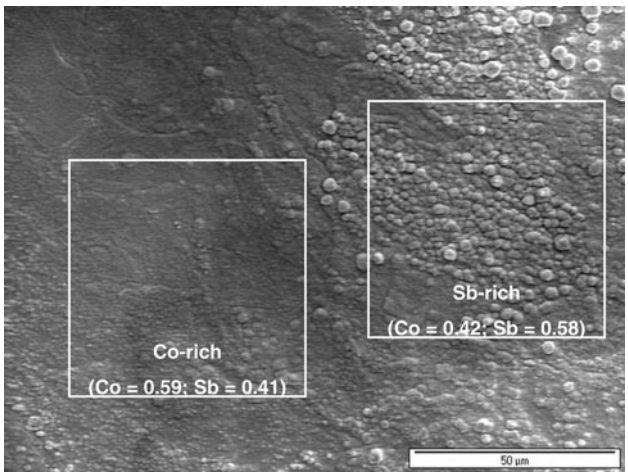

Fig. 8 SEM image of the Co–Sb surface obtained at −1.1 V for 20 min. Composition measurements from EDS are given in the area measured

composition and morphology, illustrates the interference of hydrogen evolution with the film deposition process. We have visually observed bubbles forming on the surface during deposition as the potential is set to more negative potentials, i.e., where cobalt deposits at a high rate. Once formed, these bubbles block the electrochemical reactions at the surface underneath them. Then, when the bubble detaches from the surface, it exposes an area that has a local potential slightly different from the rest of the surface. Small variations in local potential may promote the formation of a film with local variation in composition. Unlike thin film deposition, microscopic interference of hydrogen evolution in the deposition stage was not observed in the case of nanowires or overgrown nanowire (caps) films [16]. SEM has shown that nanowires grown at constant deposition potentials were sturdy and smooth, with no sign of hydrogen interference.

4 Conclusions

The electrochemical co-deposition of cobalt and antimony was studied based on a series of CV experiments at various depositions, sweep rates, and hold times. While antimony showed a characteristic peak on Au, the deposition of cobalt was far more complex and sensitive to the deposition condition. When both antimony and cobalt were co-deposited under a large overpotential, a Co–Sb compound was formed and was identified as $CoSb_3$ by XRD. However, the co-deposition was slow and could only be detected at slow sweep rate CVs.

References

1. Vining CB (2009) Nat Mater 8:83
2. Boukai AI, Bunimovich Y, Tahir-Kheli J, Yu JK, Goddard WA, Heath JR (2008) Nature 451:168
3. Hicks LD, Dresselhaus MS (1993) Phys Rev B 47:12727
4. Hicks LD, Dresselhaus MS (1993) Phys Rev B 47:16631
5. Venkatasubramanian R, Siivola E, Colpitts T, O'Quinn B (2001) Nature 413:597
6. Mi JL, Zhu TJ, Zhao XB, Ma J (2007) J Appl Phys 101:054314
7. Sales BC, Mandrus D, Williams RK (1996) Science 272:1325
8. Yan JW, Wu Q, Shang WH, Mao BW (2004) Electrochem Commun 6:843
9. Caylor JC, Stacy AM, Gronsky R, Sands T (2001) J Appl Phys 89:3508
10. Chen LJ, Hu HN, Li YX, Chen GF, Yu SY, Wu GH (2006) Chem Lett 35:170
11. Cheng H, Hng HH, Ma J, Xu XJ (2008) J Mater Res 23:3013
12. Behnke J, Prieto AL, Stacy AM, Sands T (1999) In: Proceedings of the 18th international conference on thermoelectrics, IEEE, Piscataway, p 451
13. Flis-Kabulska I (2006) J Appl Electrochem 36:131
14. Li FH, Wang W, Gao JP, Wang SY (2009) J Electrochem Soc 156:D84
15. Sadana YN, Kumar R (1980) Surf Technol 11:37
16. Quach DV, Vidu R, Groza JR, Stroeve P (2010) Ind Eng Chem Res 49:11385
17. Vidu R (2000) PhD thesis, Graduate School of Materials Engineering and Processing, Osaka University, Japan
18. Vidu R, Hara S (1999) J Electroanal Chem 475:171
19. Vidu R, Hara S (1999) Scripta Mater 41:617
20. Vidu R, Hara S (1999) Electrochemistry 67:1240
21. Vidu R, Hara S (1999) J Vac Sci Technol B 17:2423
22. Vidu R, Hara S (2000) Surf Sci 452:229
23. Vidu R, Hirai N, Hara S (2001) Phys Chem Chem Phys 3:3320
24. Hamelin A, Martins AM (1996) J Electroanal Chem 407:13
25. Jung G, Rhee C (1997) J Electroanal Chem 436:277
26. Pourbaix M (1966) Atlas of electrochemical equilibria in aqueous solutions. Pergamon Press, New York
27. Bubendorff JL, Meny C, Beaurepaire E, Panissod P, Bucher JP (2000) Eur Phys J B 17:635
28. Pandey RK, Sahu SN, Chandra S (1996) Handbook of semiconductor electrodeposition. Marcel Dekker Inc, New York
29. Abou-Krisha MM (2011) Mater Chem Phys 125:621
30. Yang ML, Hu ZB (2005) J Electroanal Chem 583:46